the plant journal

SEB SOCIETY FOR EXPERIMENTAL BIOLOGY

The Plant Journal (2021) **106,** 185–199 doi: 10.1111/tpj.15158

Unveiling the spatial distribution of aflatoxin B1 and plant defense metabolites in maize using AP-SMALDI mass spectrometry imaging

Laura Righetti[1,2,*], Dhaka Ram Bhandari[2], Enrico Rolli[3], Sara Tortorella[4], Renato Bruni[1], Chiara Dall'Asta[1] and Bernhard Spengler[2,*]

[1]*Food and Drug Department, University of Parma, Viale delle Scienze 17/A, Parma 43124, Italy,*

[2]*Institute of Inorganic and Analytical Chemistry, Justus Liebig University Giessen, Heinrich-Buff-Ring 17, Giessen 35392, Germany,*

[3]*Department of Chemistry, Life Sciences and Environmental Sustainability, University of Parma, Via G.P. Usberti 11/a, Parma 43124, Italy, and*

[4]*Molecular Horizon Srl, Via Montelino 30, Bettona, Perugia 06084, Italy*

Received 5 July 2020; revised 25 October 2020; accepted 24 November 2020; published online 9 January 2021.
*For correspondence (e-mail laura.righetti@unipr.it; Bernhard.Spengler@anorg.chemie.uni-giessen.de).

SUMMARY

In order to cope with the presence of unfavorable compounds, plants can biotransform xenobiotics, translocate both parent compounds and metabolites, and perform compartmentation and segregation at the cellular or tissue level. Such a scenario also applies to mycotoxins, fungal secondary metabolites with a pre-eminent role in plant infection. In this work, we aimed to describe the effect of the interplay between *Zea mays* (maize) and aflatoxin B1 (AFB1) at the tissue and organ level. To address this challenge, we used atmospheric pressure scanning microprobe matrix-assisted laser desorption/ionization mass spectrometry imaging (AP-SMALDI MSI) to investigate the biotransformation, localization and subsequent effects of AFB1 on primary and secondary metabolism of healthy maize plants, both *in situ* and from a metabolomics standpoint. High spatial resolution (5 μm) provided fine localization of AFB1, which was located within the root intercellular spaces, and co-localized with its phase-I metabolite aflatoxin M2. We provided a parallel visualization of maize metabolic changes, induced in different organs and tissues by an accumulation of AFB1. According to our untargeted metabolomics investigation, anthocyanin biosynthesis and chlorophyll metabolism in roots are most affected. The biosynthesis of these metabolites appears to be inhibited by AFB1 accumulation. On the other hand, metabolites found in above-ground organs suggest that the presence of AFB1 may also activate the biochemical response in the absence of an actual fungal infection; indeed, several plant secondary metabolites known for their antimicrobial or antioxidant activities were localized in the outer tissues, such as phenylpropanoids, benzoxazinoids, phytohormones and lipids.

Keywords: plant defense metabolites, mass spectrometry imaging, aflatoxins, metabolomics, phytotoxicity, *Zea mays*.

INTRODUCTION

Plants are sessile organisms, with the capability to adapt and thrive that is mediated by an ability to interact with their surroundings and provide optimal responses to multiple stimuli and threats. Such versatility is also the result of an intricate chemical interplay with other organisms, including the regular exchange of organic compounds that can be both released in the rhizosphere or taken up by the roots (Jones *et al.*, 2009; van Dam and Bouwmeester, 2016). This bidirectional flow involves substances modulating soil microbiota, providing kin recognition between plants or eliciting a variety of physiological and metabolic responses. Besides allowing the uptake/release of carbon or nitrogen, it also involves plant and microbial secondary metabolites (Buer *et al.*, 2007; Biedrzycki and Bais, 2010; Bonfante and Genre, 2010; Zhalnina *et al.*, 2018). The overall consequence is the evolutionary result of conflicting needs, a dynamic balance between the advantages of increased environmental control and the drawbacks of xenobiotics causing unwanted effects on plant metabolism. Like any other system of this kind, chemical signaling pathways at the soil–root interface can be hijacked by third parties to alter plant

physiology in order to gain some sort of advantage (Venturi and Keel, 2016). This form of hijacking has been reported in a variety of species affected by the radical uptake of cyanobacterial microcystins and benzoxazinones or strigolactones produced by other plants for allelopathic purposes (Peuthert *et al.*, 2007; Crush *et al.*, 2008; Schulz *et al.*, 2013). Thought of as an adaptation to the evolutive pressure exerted by these substances, the absorption of specific chemical compounds is also known to act as an alert system in plants, eliciting precise metabolic responses, such as activating pathways that lead to the increased biosynthesis of defensive metabolites or the expression of enzymatic pools responsible for xenobiotic degradation of any origin (Siminszky, 2006; D'Abrosca *et al.*, 2013). To cope with the absorption of unfavorable compounds, plants are thus capable to biotransform xenobiotics, translocate both parent compounds and metabolites, and perform compartmentation and segregation at the cellular or tissue level in organs programmed for senescence (Schröder and Collins, 2002; Herzig *et al.*, 2011).

Such a scenario also applies to the heterogeneous class of mycotoxins, fungal secondary metabolites produced by genera involved in plant pathology and food spoilage, such as *Alternaria*, *Aspergillus*, *Fusarium* and *Penicillium*. Being hemibiotrophic pathogens, these fungi produce toxins known in some cases to hijack their host secondary metabolic pathways. Until now, the role of these pathogens has mostly been described during the necrotrophic phase (Perincherry *et al.*, 2019). A phytotoxic role has been defined for deoxynivalenol (DON) and alternariol, along with a potential role as a virulence factor during an actual infection, facilitating the colonization of host plants by *Fusarium* and *Alternaria* spp. (Proctor *et al.*, 2002; Wenderoth *et al.*, 2019; Wipfler *et al.*, 2019). At the same time, growing evidence shows that most mycotoxins, including aflatoxins, ochratoxins, patulin, citrinin and fumonisins, can be absorbed by roots and translocated to above-ground organs, as noted in asymptomatic *Arachis hypogaea* (peanut), *Asparagus officinalis* (asparagus), *Coffea arabica* (coffee), *Lactuca sativa* (lettuce), *Oryza sativa* (rice), *Saccharum officinarum* (sugarcane) and *Zea mays* (maize) crops (Mertz *et al.*, 1980; Llewellyn *et al.*, 1982; Walker *et al.*, 1984; Snigdha *et al.*, 2015; Hariprasad *et al.*, 2015). More recently, the uptake, biotransformation and distribution of zearalenone, DON, T2 toxin and HT-2 toxin in different plant organs was demonstrated in healthy maize and *Triticum aestivum* (wheat) plants, confirming that the biochemical response of plants is also activated in the absence of an actual fungal infection (Righetti *et al.*, 2017; Rolli *et al.*, 2018; Righetti *et al.*, 2019). It is not yet known if such a phenomenon, occurring in healthy plants exposed to substances released by fungi in the soil, is somewhat involved in plant resistance or fungal attack strategies. It is instead known that the plant response to xenobiotics is the consequence of regioselective and stereospecific reactions mediated by P450 cytochromes and actuated by the differential distribution of their products, resulting in a dynamic and variable portfolio of structures defined as the 'xenobolome'. Our understanding of the xenobolome has been greatly increased by the availability of metabolomic techniques, such as those based on mass spectrometry, with a growing number of so-called 'masked' or 'modified' mycotoxins obtained *in planta* (Berthiller *et al.*, 2013; Rychlik *et al.*, 2014; Zhang *et al.*, 2019).

At present the literature is most focused on the description of the chemical diversity of the xenobolome, however, and limited information is available regarding the correlation between plant tissues, uptake, biotransformation and distribution, without taking full advantage of modern analytical tools like those made available by mass spectrometry imaging (MSI). For instance, despite the growing number of plant metabolites of mycotoxins described, we currently do not have indications about fundamental aspects relevant for a proper understanding of the plant response to aflatoxin exposure: the weakening or stimulating effect on plant primary or secondary metabolism and the absorption dynamics of aflatoxins or their modified forms in different tissues and organs. Aflatoxin B1 (AFB1) in particular is the most potent and abundant difuranocoumarin-based secondary metabolite produced by *Aspergillus flavus* and *Aspergillus parasiticus*. As a result of the combination of carcinogenicity and distribution, AFB1 represents a serious issue in food chains, but is also produced in surface soil in the presence of maize residues, and may therefore be involved in crosstalk between plants and fungi at the root level (Accinelli *et al.*, 2008).

In this regard, modern metabolomics coupled with MSI may allow for a better insight into the interplay between plants and mycotoxins, highlighting potential variations in distribution and biotransformation between different tissue and cell types. The fine combination of chemical and histological data may not only elucidate the molecular entities involved in these processes but also their spatial distribution within the organism (Boughton *et al.*, 2016). Atmospheric pressure scanning microprobe matrix-assisted laser desorption/ionization (AP-SMALDI) MSI, for instance, is versatile enough to cover a broad range of plant natural products. Recently it has been applied to the metabolic effects of biotic and abiotic stress (Bhandari *et al.*, 2018) or to the simultaneous localization of multiple secondary metabolites and xenobiotics, also at the cellular level, but has never been used before to describe the consequences of mycotoxins in living plants, including those related to AFB1 (Tenenboim and Brotman, 2016; Villette *et al.*, 2019).

Here, we present an initial attempt to describe the effects of the interplay between plants and aflatoxins at the tissue and organ level in the most common and relevant

mycotoxins produced by some *Aspergilli* species and strains. We used AP-SMALDI MSI *in situ* and from a metabolomics standpoint to investigate the biotransformation, distribution, localization and subsequent effects of AFB1, and its potential modified forms, on primary and secondary metabolism of healthy maize plants.

RESULTS

MALDI matrices for aflatoxin ionization

Given the limited availability of *ad hoc* MSI methods for aflatoxins (de Oliveira *et al.*, 2014; Hickert *et al.*, 2016), an optimization of ionization and detection parameters for AFB1 was performed. The matrices α-cyano-4-hydroxycinnamic acid (CHCA) and 2,5-dihydroxybenzoic acid (DHB), and different combinations of solvents, were tested with the AFB1 standard (1 μg ml^{-1}). CHCA (50% acetonitrile) yielded the best signal in the dried-droplet MALDI experiment, in agreement with Hickert *et al.* (2016); however, when performing on-tissue MSI, DHB (50% acetone) provided the highest signal for AFB1. Consequently, DHB was chosen as the matrix for MALDI-MSI experiments with maize samples. Note that DHB is also appropriate for detecting plant metabolites at high sensitivity in positive-ion mode (Bjarnholt *et al.*, 2014; Bhandari *et al.*, 2015), and thus is also suitable to detect variations in the plant metabolome in response to AFB1 exposure.

AFB1 localization in maize root

Simultaneous analysis of tissue sections of control and AFB1-treated roots was performed. Both samples were mounted on the same glass slide and acquired on the same analytical run to minimize technical error, and thus intersample variability.

In our experiment, plant roots were fully immersed in medium containing AFB1 for 7 and 14 days. The intact plantlets rapidly took up the AFB1, which was completely removed from the medium after 14 days and was almost 90% absorbed after 7 days, confirming previous studies reporting root uptake and translocation to above-ground organs in asymptomatic *Z. mays* (Mertz *et al.*, 1980). The percentage of AFB1 uptake from the medium was determined by ultra-high-performance liquid chromatography (UHPLC) high-resolution tandem mass spectrometry (HRMS/MS) analysis (Appendix S1; Figure S1).

After 7 days of treatment, images from AP-SMALDI measurements (see Figure S2) show the spatial distribution of AFB1, accumulated in epidermal root cells. The AFB1 distribution changed in roots treated for 14 days, indicating time-dependent root uptake. Compared with the shorter treatment (Figure S2), AFB1 was detected spreading in the cortex cells and in the root stele (see Figure 1a), suggesting its distribution through the xylem vessels and a potential translocation to the aerial parts of the plantlet. AFB1 was detected exclusively in the treated root and not in the control sample, as shown in Figure 1(a), thereby confirming the identity of the molecule despite the lack of HRMS/MS data caused by the weak signal intensity. AFB1 was detected as protonated, sodium or potassium adducts, with the latter giving the highest intensities. The three adducts showed the same spatial distribution.

The UHPLC HRMS/MS using the authentic standard compound supported the results of the AP-SMALDI MSI.

Upon entry to plant tissues, AFB1 seems to undergo a fate similar to most xenobiotics, being biotransformed by the plant enzymatic pool involved in detoxification, with the production of so-called masked mycotoxins. Our AP-SMALDI MSI data confirmed such a hypothesis and, for instance, aflatoxin M2 (AFM2) was found to be the most abundant metabolite. Indeed, AFM2 was already detected after 7 days of treatment and was co-localized with AFB1. AP-SMALDI imaging results (Figure S2) indicated that AFM2 mainly accumulates in the epidermis, suggesting co-localization with the pool of enzymes capable of converting AFB1 into AFM2. As for AFB1, in the root treated for 14 days the localization of AFM2 changed, spreading throughout the cortex cells (Figure 2). AFM2 identification was confirmed by comparison with the analytical standard by running the same sample using UHPLC HRMS/MS (Figure S3). Sample preparation and UHPLC HRMS/MS analysis are described in Appendix S1.

Distribution images of AFB1 and its metabolite AFM2 were obtained exclusively from the root, whereas in the stem and leaf organs their ion intensities were below the limit of detection of AP-SMALDI MSI. Indeed, the majority of the 200 μg of AFB1 spiked in the growing medium accumulated in the root (63%), whereas only a smaller quantity was translocated through the stem (34%) and leaves (3%) (Figure S1). This accumulation in the root is to be expected, as the growing medium was spiked with AFB1 and thus AFB1 entered the plant through root uptake. The translocation of AFB1 and AFM2 to the aerial part of the plantlets is likely to occur as previously demonstrated (Mertz *et al.*, 1980), and was confirmed by UHPLC HRMS/MS analysis (Appendix S1; Figure S1).

Evidence for apoplastic uptake and storage of aflatoxins

The detoxification of xenobiotics in the plant, including mycotoxins, has been suggested to occur in the Golgi apparatus, followed by the release of the metabolites into the apoplast via exocytosis (Coleman *et al.*, 1997).

Based on our results, AFB1 uptake followed the apoplastic route, through the interconnected cell wall spaces. Based on the image with 5-μm resolution (see Figure 3), zoomed in and enlarged for better visualization, it was found that AFB1 was located within the intercellular spaces, outside of the outermost layer of the cell walls, which was not discernable at 10 μm (Figure 1a). This

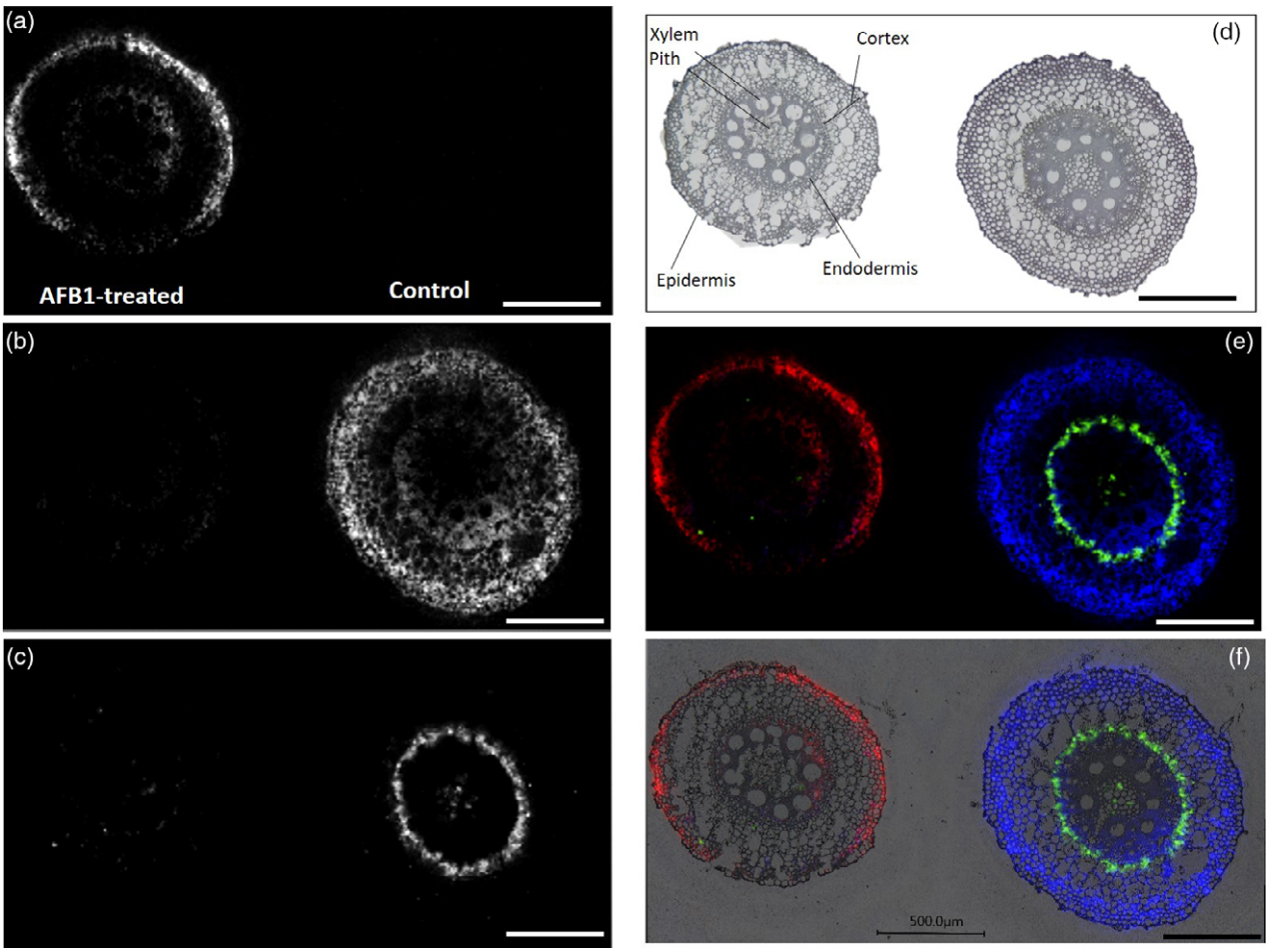

Figure 1. AP-SMALDI mass spectrometry imaging of control and AFB1-treated *Zea mays* (maize) root sections after 14 days of the experiment. (a) Aflatoxin B1 $[M + K]^+$, *m/z* 351.0265, is accumulated in the epidermis cells and in the cortex cells. (b) Cyanidin glucoside $[M]^+$, *m/z* 449.1076, and (c) pheophytin a $[M + H]^+$, *m/z* 871.5729, spatial distribution in root. (d) Optical image of AFB1-treated and control maize root sections, with major morphological features labeled. (e) Red–green–blue (RGB) overlay image of AFB1 $[M + K]^+$, *m/z* 351.0265 (red), pheophytin a $[M + H]^+$, *m/z* 871.5729 (green), and cyanidin glucoside $[M]^+$, *m/z* 449.1076 (blue). (f) RGB metabolite image, overlain with the optical image. All images are normalized to the total ion current on a 0–70% intensity scale. MS images of maize roots were generated with 295 × 145 pixels, with a pixel size of 10 μm and an *m/z* bin width of ±5 ppm. Scale bars: 500 μm.

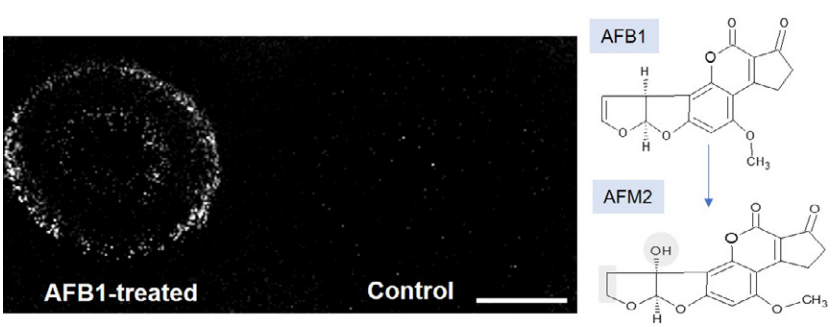

Figure 2. AFM2 distribution after 14 days of treatment. AFM2 $[M + K]^+$, *m/z* 369.0371, was found to be located mainly within the epidermis and cortex cells. The image was normalized to the total ion current on a 0–50% intensity scale. The MS image of maize root was generated with 295 × 145 pixels, with a pixel size of 10 μm and an *m/z* bin width of ±5 ppm. Scale bar: 500 μm.

demonstrates the necessity of high resolution for the elucidation of fine localization information. This distribution pattern is more evident at this resolution, especially when overlain with the optical images (see Figure 3).

Individual cell walls can be observed within the epidermis (7 days root) and cortex (14 days root) layers using 5-μm resolution, as shown in Figure 3. These cells have a diameter of around 30 μm, and therefore measurement

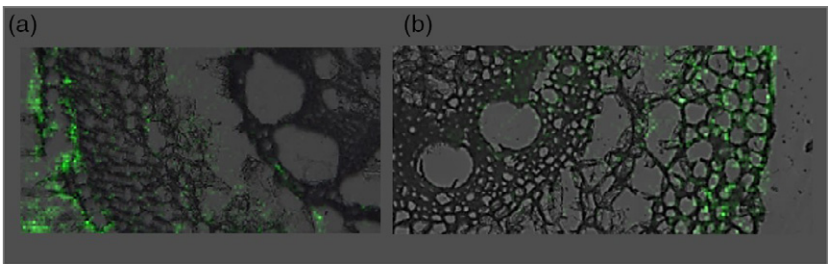

Figure 3. Magnified ion images of AFB1 in maize root after 7 days (a) and after 14 days (b). AFB1 $[M + K]^+$, *m/z* 351.0265 (green), accumulated in the epidermis cell wall (a), and after 14 days was located within the cortex cells in the root apoplast. MS images of maize root were generated with: (a) 177 × 191 pixels, with a pixel size of 5 μm and an *m/z* bin width of ±5 ppm; (b) 230 × 240 pixels, with a pixel size of 5 μm and an *m/z* bin width of ±5 ppm.

with a lateral resolution of 5 μm was adequate to obtain fine localization information by retaining enough signal intensity.

Location of metabolites involved in the defense against aflatoxin accumulation

Plant changes induced by aflatoxin accumulation have been investigated, mainly using genomics and transcriptomics, whereas the effects on plant metabolism and thus the metabolic response of plants to such exposure are poorly studied. Here, we applied an untargeted MSI-based metabolomics workflow to visualize changes in the maize metabolome following AFB1 accumulation.

At first, exploratory unsupervised data mining, including principal components analysis (PCA) and segmentation analysis, was performed. PCA was applied to the pre-processed data to identify discriminating *m/z* values and to detect underlying structures based on similarities or differences among the pixel-based mass spectra (Kulkarni *et al.*, 2018). Significant metabolites involved in the defense mechanism were selected from the resulting loading plots. Root, stem and leaf samples were processed independently, considering that AFB1 is expected to exert different phytotoxicity on the three studied organs, depending on the extent of its AFB1 accumulation in tissue. Therefore, the location of metabolites involved in the defense against aflatoxin accumulation is discussed accordingly. The metabolites detected in the different maize organs and those discussed throughout the article are listed in Table 1. Additional discriminant metabolites are reported in Table S2.

Table 1 Selected metabolites assigned in *Zea mays* (maize) organs by AP-SMALDI MS, the *m/z* images of which are presented in the figures

Subclass	Compounds	Molecular formula	Adduct	Exact mass	Error ppm	Localization (organ)	Higher metabolite intensity in	Identification level[a]
Furanocoumarins	AFB1	$C_{17}H_{12}O_6$	$[M + K]^+$	351.0265	0.83	Epidermis and cortex (root)	AFB1-treated	I
Furanocoumarins	AFM2	$C_{17}H_{14}O_7$	$[M + K]^+$	369.0371	0.8	Epidermis and cortex (root)	AFB1-treated	I
Chlorins	Pheophytin a	$C_{55}H_{74}O_5N_4$	[M]+	871.5732	0.62	Endodermis (root) mesophyll (leaf)	Control sample	II
Flavonoid glycosides	Cyanidin glucoside	$C_{21}H_{21}O_{11}$	$[M]^+$	449.1078	0.57	Cortex cells (root)	Control sample	III
Steroid lactones	Deoxybrassinolide	$C_{28}H_{48}O_5$	$[M + K]^+$	503.3133	0.01	Leaf epidermis (stem)	AFB1-treated	III
Carbohydrates and carbohydrate conjugates	HDMBOA-Glc	$C_{16}H_{21}NO_{10}$	$[M + H]^+$	388.1238	1.09	Leaf sheath (stem)	AFB1-treated	III
Glycosyldiacylglycerols	DGDG (34:2)	$C_{49}H_{88}O_{15}$	$[M + Na]^+$	939.6015	0.2	Collenchyma (leaf)	AFB1-treated	III
Flavonoid glycosides	Malvidin	$C_{17}H_{15}O_7$	[M]+	331.0812	0.8	Vascular tissue (leaf)	Control sample	II

[a]Level of metabolite identification according to the Metabolomics Standard Initiative (Schymanski *et al.*, 2014): I, confirmed structure by reference standard; II, probable structure by library spectrum match; III, tentative candidate.

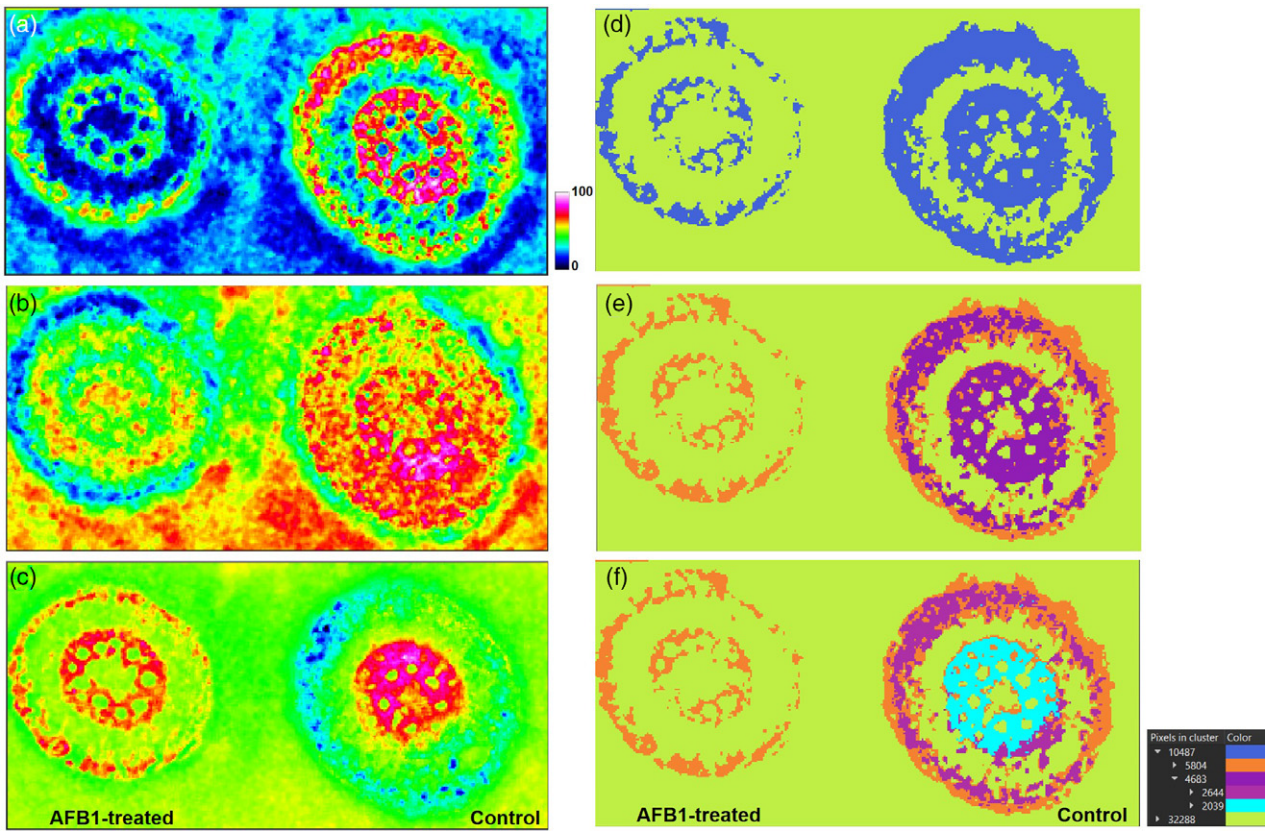

Figure 4. Exploratory data analysis for AP-SMALDI imaging of a maize root sample to visualize inter- and intra-sample comparison. Two unsupervised approaches are compared: (a–c) principal component analysis (PCA); and (d–f) bisecting *k*-means segmentation. (a–c) PCA-score images of the first (a), second (b) and third (c) principal components. Images scaled to 0–100% score and displayed with a rainbow color gradient (black, low values; white, high values). (d–f) Segmentation clusters expanded to the first (d), second (e) and third (f) layers. At the first iteration (d), the out-of-tissue (yellow) and in-tissue (blue) clusters were identified. At the second and third iterations, the distinct clusters correlate with root histology, such as epidermis (orange cluster), cortex (blue and violet cluster) and pith (cyan cluster). The hierarchy relations between clusters are shown in the legend.

Roots

Plant roots are actively involved in plant–environment interactions at the soil level, and both their structure and metabolism are the result of a series of necessary compromises between two opposite necessities: the uptake of water, nutrients and chemical signals; and the defense against biotic and abiotic stress. Therefore, changes of endogenous metabolites in different root regions are essential to reveal the adaptation mechanisms. Roots are composed of a variety of tissue types on a small scale (e.g. xylem, phloem, cortex and pith; see Figure 1d), and high spatial resolution is crucial for the mapping of chemical distribution at the cellular level. In particular, root samples were acquired using a pixel size of 10 μm, and analyses were repeated with a higher spatial resolution (5 μm) to obtain fine localization information for certain metabolites.

Simultaneous analyses of control and AFB1-treated roots were performed, by mounting both samples on the same glass slide.

To perform PCA (see Figure 4a–c), we selected three principal components (PCs) based on the total variance captured (92%). PC1 captures 73% of the total variation, whereas combined PC2 and PC3 explain a total of 19%. As shown in Figure 4, the score images for PC1, PC2 and PC3 show an enhanced chemical contrast between the treated and the control root. In addition, the score images of PC1 and PC2 capture the variation in intensity arising from the histology of the root surface, which includes the outer epidermis and the pith.

In parallel, segmentation analysis was performed revealing different regions of interest (ROIs) (Figure 4d–f). The first layer expansion (Figure 4d) discriminates out-of-tissue (green cluster) and in-tissue (blue cluster) signals, whereas the second (Figure 4e) and third cluster layers (Figure 4f) nicely distinguish between plants treated with AFB1 and the controls. Furthermore, the distinct clusters strongly correlate with the root tissue compartments, such as the epidermis (orange cluster), cortex (violet cluster) and pith (cyan cluster).

Overall, the output from both unsupervised exploratory approaches reported consistent results, revealing the hidden differential metabolic distribution profiles between control and treated roots, and defining important compartmentation regions at the plant tissue level. It should be mentioned that PCA and segmentation are independent analyses that are based on different algorithms, and thus the consistency in the results suggest a significant difference in the metabolic profile of control and treated roots.

Subsequently, five ROIs for each cluster were generated and underwent further multivariate statistical analysis, namely PCA (with the score plot reported in Figure S4).

A grouping of samples according to treatment, following the direction of the first PC (Figure S4), whereas the second PC better explained intra-sample variation arising from different tissues. Therefore, PC1/PC2 loading plots were investigated to isolate metabolites differentially accumulated and distributed in mycotoxin-treated samples versus control samples.

Chlorophylls seem to be particularly affected by the presence of AFB1. Indeed, several derivates including pheophytin a, pheophytin b, chlorophyllide a and chlorophyllide b were detected exclusively in control roots, thus suggesting degradation or inhibited synthesis in plantlets exposed to AFB1 (Table 1). This remarkable inhibitory effect on chlorophyll synthesis was reported previously in maize (McLean *et al.*, 1992) and other crops (McLean *et al.*, 1995; Ismaiel and Papenbrock, 2015) treated with AFB1.

These compounds appear to be co-localized in the endodermis cell layer (Figures 1 and S5; for compound identification, see Figure S6). The site of accumulation of chlorophylls in the root is consistent with results previously obtained in illuminated Arabidopsis roots as a consequence of a precise cytokinin/auxin ratio (Kobayashi *et al.*, 2012); however, their biosynthesis in plantlets treated with AFB1 may suggest a direct or indirect capability to disrupt such activity in maize, at least *in vitro* where roots are exposed to light.

A similar trend but a different localization was observed for anthocyanidin compounds. The predominant anthocyanidins found in roots of untreated plantlets were malvidin, cyanidin-malonylglucoside and peonidin glucoside, followed by cyanidin glucoside and pelargonidin glucoside. These compounds are known to be present in maize and are known for their involvement in a variety of stress-related responses in plants, and in monocots in particular (Salinas Moreno *et al.*, 2005). Along with other flavonoids, anthocyanins may act as phytoanticipins, and therefore may be transformed into more active substances (phytoalexins) when plants are under threat from microorganisms. At the same time, they are overproduced when plants suffer drought, cold or exposure to UV light. Their reduced biosynthesis in AFB1-treated samples and the apparent lack of related phytoalexins may suggest a possible weakening of the defensive system of maize exerted by AFB1.

As noted for chlorophylls, variations in anthocyanidin levels were reported with several compounds exclusively found in the control root, showing accumulation in the root cortical parenchyma, but not in plantlets treated with AFB1. In particular, cyanidin glucoside ($[M]^+$ *m/z* 449.1076) was found to be exclusively present in the control root, showing accumulation mainly in the root parenchyma cortex cells (see Figure 1b).

Co-localized ion signals were extracted, highlighting several features sharing the same distribution and trend regarding treatment. The MS images of these features, most likely anthocyanidin-like metabolites, are collected in Figures S7 and S8.

Stems

Stems are a part of the shoot plant system with support and transport functions. The plant stem not only helps to transport absorbed water and minerals but also the products of photosynthesis and metabolism. Thus, detailed knowledge on metabolite distribution in the maize stem is fundamental for the understanding of molecular transport and nutrient storage networks. As in maize, the lower part of each leaf encloses the stem, forming a leaf sheath, with three main structures: the stem pith, the leaf sheath and the vascular bundles (for an optical image with the major morphological features labeled, see Figure 4d). In contrast to root, considering the stem diameter (approximately 2 mm) and the morphological organization, a pixel size of 30 μm was used in MSI experiments. A higher resolution would have led to lower signal intensities and significantly increased acquisition times.

As for the roots, exploratory data analysis was performed and the resulting PCA and segmentation analysis are reported in Figures S9 and S10. The result from the PCA shows a sample clustering, influenced both from the treatment and the tissue, suggesting a less significant effect of AFB1-induced stress compared with the root (Figure S10). Consistent with this, AFB1 accumulation in the stem (34%) was lower than in the roots (63%) (Figure S1). All these observations correlate with the assumption of compartmentalized metabolism in plants among different organs.

Compared with roots, few significant metabolites selected from the loading plot were found to be modulated by treatment with AFB1. This is likely to be a consequence of the lower accumulation of aflatoxins resulting from the diluting and dynamic effects of transportation.

The MSI measurement demonstrated the fine localization of constitutive and defense-related metabolites. Distribution of monogalactosyldiacylglycerol 36:6 (MGDG) (Figure 5a) was found to be not affected by the treatment, and its ion image correlates well with the optical image

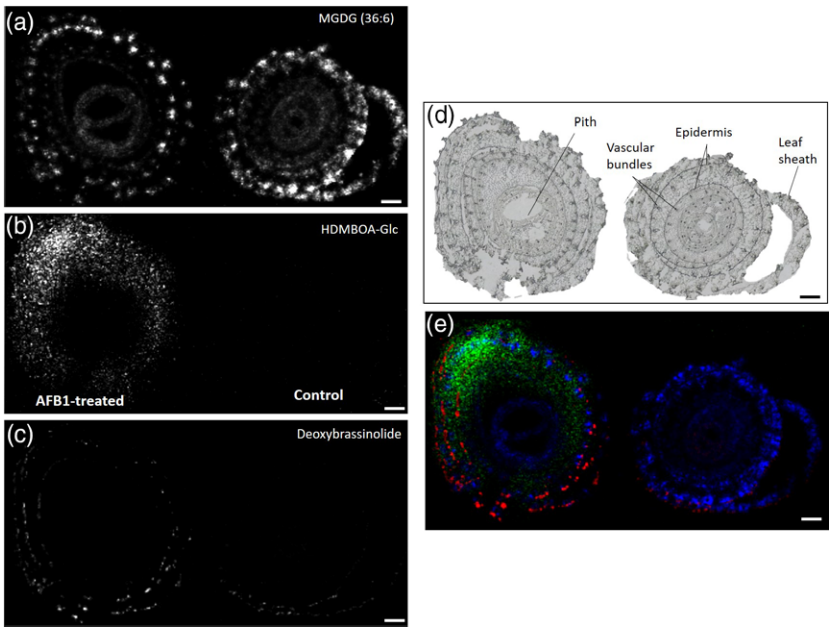

Figure 5. AP-SMALDI mass spectrometry imaging of AFB1-induced defense-related metabolites in the stem (a–c). (a) MGDG (36:6) $[M + K]^+$, *m/z* 813.4914, was found to be widespread in both control (right) and treated (left) stems. HDMBOA-Glc (b) and deoxybrassinolide (c) were found to be present in the outer leaf sheath of the treated stem. In particular, HDMBOA-Glc $[M + H]^+$, *m/z* 388.1234, accumulated in the leaf sheath, whereas deoxybrassinolide $[M + K]^+$, *m/z* 503.3133, was found to be enriched in the vascular bundles of the leaf sheath. (d) Optical image of AFB1-treated versus control maize stem sections, with major morphological features labeled. (e–f) Overlay image of MGDG (36:6), *m/z* 813.4914 (blue), HDMBOA-Glc $[M + H]^+$, *m/z* 388.1234 (green), and deoxybrassinolide $[M + K]^+$, *m/z* 503.3133 (red). All images were normalized to total ion current on a 0–70% intensity scale. MS images of the maize stem were generated with 338 × 172 pixels, with a pixel size of 30 μm and an *m/z* bin width of ±5 ppm. Scale bars: 500 μm.

(Figure 5d). In contrast, defense compounds, including hydroxydimethoxy benzoxazinone glucoside (HDMBOA-Glc) (Figure 4b) and deoxybrassinolide (Figure 4c) were found to be differentially distributed among control and treated stems, and were located in the outer tissues. Both metabolites were exclusively found in the AFB1-treated stems.

HDMBOA-Glc ($[M + H]^+$ *m/z* 388.1234) belongs to the benzoxazinoids, which are secondary plant metabolites, widely acknowledged for their importance in plant defense in both above- and below-ground parts of cereal plants (Zhou *et al.*, 2018). The compound was found accumulated in the mesophyll cells of the AFB1-treated leaf sheath. Instead, deoxybrassinolide ($[M + K]^+$ *m/z* 503.3133) was found to be enriched in the vascular bundles of AFB1-treated leaf sheath. This compound belongs to the new class of phytohormones with protective effects, growth effects, chlorophyll biosynthesis and membrane stability in maize (He *et al.*, 1991).

Additional metabolites associated with stem defense against AFB1 accumulation are shown in Figure S11.

Leaves

A wide range of processes takes place simultaneously in leaves, including transpiration, respiration, plant–pathogen interaction and plant defense. Considering the morphological organization of a leaf, a pixel size of 10 μm was chosen for MSI acquisition.

In this case, it was not possible to mount both treated and control samples on the same glass slides, because of the fragility of the tissue. To obtain uniform sections, adhesive tape was used over the trimmed sample during the cryosectioning step.

The presence of AFB1 in the leaf of treated maize plantlets was assessed using UHPLC HRMS/MS analysis. Only 3% of the total AFB1 administered to the medium was translocated to the leaf organ (Figure S1). Consistent with this, few differences in the metabolome profile were identified, as suggested also by the result of the exploratory data analysis reported in the Figures S12 and S13.

As shown in Figure 6, the distribution of pheophytin a (Figure 6c,d) was homogeneous, regardless of the treatment, and accumulated in the mesophyll cells. This localization is consistent with the results described previously for healthy maize leaves (Dueñas *et al.*, 2017).

In contrast, digalactosyl diacylglycerol (DGDG) (34:1) (Figure 6e,f) and malvidin (Figure 6g,h) were found to be differentially accumulated in response to AFB1 treatment. Malvidin was found to be reduced in the bundle sheath of treated leaves, whereas DGDG (34:1) was stored in the collenchyma of the treated leaf. Alterations and remodeling in galactolipid composition were recently studied in two

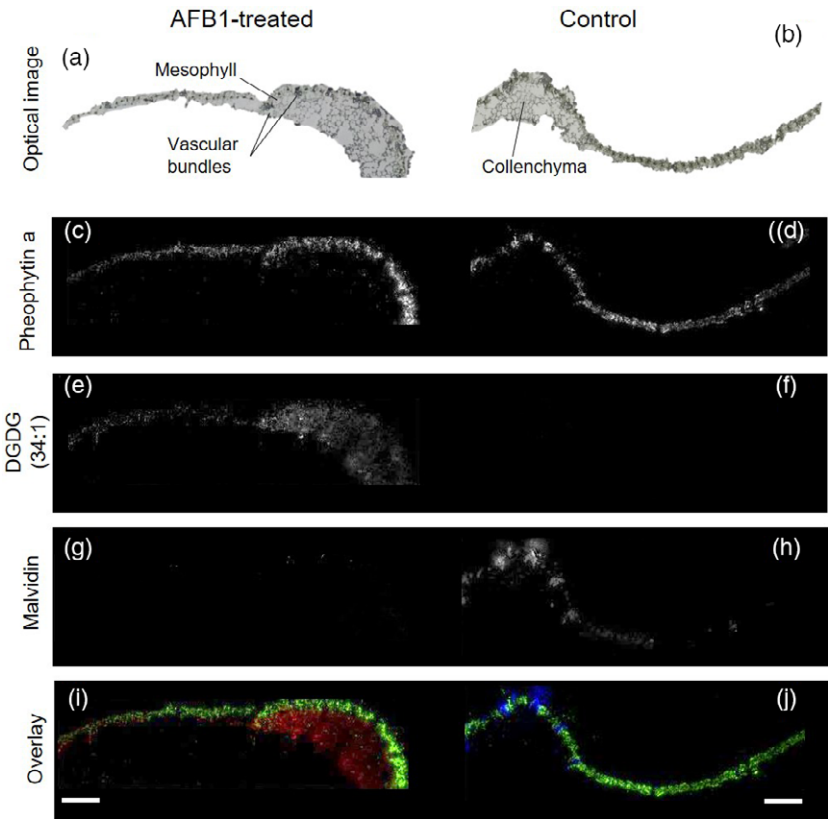

Figure 6. Optical images of maize leaf sections, with major morphological features labeled (a, b). AP-SMALDI mass spectrometry imaging of AFB1-induced defense-related metabolites in leaves (c–h). (i–j) RGB overlay image of DGDG (34:1), *m/z* 939.6017 (red), pheophytin a $[M + K]^+$, *m/z* 909.5291 (green), and malvidin $[M]^+$, *m/z* 331.0814 (blue). All images were normalized to total ion current on a 0–60% intensity scale. MS images of maize leaves were generated with 388 × 172 pixels, with a pixel size of 30 μm and an *m/z* bin width of ±5 ppm. Scale bars: 500 μm.

maize cultivars differing in drought-induced leaf senescence (Chen *et al.*, 2018), suggesting an increase of the galactolipid DGDG during leaf stress. Furthermore, the accumulation of DGDG leads to an increase in the DGDG/MGDG ratio, which may help to maintain the chloroplast membrane in the bilayer conformation, necessary for its biological functions (Chen *et al.*, 2018).

DISCUSSION

Metabolic changes occur when plants are exposed to xenobiotics, providing both localized and systemic responses. Here, MSI was employed to simultaneously explore the spatiotemporal distribution and the metabolic fate of AFB1, its putative modified forms (masked mycotoxins), and plant-stress metabolites induced by their accumulation in different cells, tissue and organs. In other words, a visualization of how and where maize biotransforms AFB1 after physiological uptake was provided, and the resulting changes to the plant metabolome were described.

Following radical uptake by maize plantlets, AFB1 was absorbed from the growing medium after 14 days, accumulated in the root, translocated through stem and leaf, and metabolized. AFB1 is indeed recognized by the plant as a xenobiotic, exhibiting phytotoxicity, and thus is metabolized into less toxic forms, with among others AFM2 as the oxidized form of AFB2.

Xenobiotic residues resulting from phase I (transformation) and phase II (conjugation) are usually segregated in vacuoles or accumulated in the apoplast (phase III), including cell wall bonding. In our study, the distribution of AFB1 elucidated by high spatial resolution MSI is consistent with an earlier hypothesis on the compartmentalization of mycotoxins (Coleman *et al.*, 1997). Indeed, our results indicate that after 14 days AFB1 is mostly found in the root apoplast, and its distribution to above-ground organs is at least slowed by this organ, probably allowing the whole plant a longer time to prepare against potential fungal infection. Other xenobiotics, including herbicides, pesticides, fungicides (i.e. atrazine, fenapanil, fenarimol, glyphosate and oxamyl) and host-selective toxin Ptr ToxB have been detected before in the plant apoplast, but their distribution has been traditionally investigated using immunocytochemical methods (i.e. fluorescence microscopy) (Martin and Edgington, 1981; Jachetta *et al.*, 1986;

Figueroa *et al.*, 2015; Bártíková *et al.*, 2015). Here, we disclose the exact location of AFB1, taking advantage of the MSI capabilities, including the use of high spatial resolution MSI. Not only AFB1 but also its metabolite AFM2 was co-localized in the root apoplast. This result suggests that AFB1 is sensitive to enzymatic pools present in the root apoplast (Nelson, 2006). In mammals, AFB1 undergoes a variety of modifications in the liver under the action of the superfamily of CYP450 microsomal enzymes, and particularly through the mixed-function oxidase enzymes. For instance, their activity induces the hydroxylation necessary to obtain AFM1, and therefore similar enzymes may be involved in the conversion observed in maize roots. As a rule of thumb, the extent of apoplast accumulation of a given compound is considered to be a consequence of several parameters (i.e. osmotic potential, pH, charge, partitioning coefficient, carriers): among these, water solubility slows down penetration in the symplast (Martin and Edgington, 1981; Jachetta *et al.*, 1986; Meinzer and Moore, 1988). Therefore, a distinct behavior might be expected for mycotoxins with different polarities, such as zearalenone, a lipophilic mycotoxin. Indeed, distinct distributions were reported for herbicides with different solubilities. Atrazine (water solubility = 33 mg L^{-1}; log $P = 2.6$) has been demonstrated to penetrate the symplast of maize root tissue (Jachetta *et al.*, 1986), whereas glyphosate (water solubility = 10 g L^{-1}; log $P = -3.4$) remains in the apoplast.

The findings presented here suggest that AFB1 may act as an extracellular effector localized in plant extracellular spaces, a chemical presence that maize plants may consider as a potential risk even when no infection is present. This result, albeit obtained in a simplified system, might represent a step towards a better understanding of the role of these natural toxins in disease susceptibility and modulation of pathogenesis when fungal species are also present. How AFB1 is transported remains to be examined, however, and whether at given conditions AFM2 may be present in significant quantities in aerial organs. At the same time, the recourse to an *in vitro* approach, relying on radical uptake and on leaf transpiration for systemic distribution of AFB1 and its metabolites, may depict a different scenario from that present when maize ears or aerial organs are actually infected by *Aspergillus* fungi.

We provided a parallel visualization of maize metabolic changes, induced in different organs and tissues by an accumulation of AFB1. Mycotoxins may also activate the biochemical response of plants in the absence of an actual fungal infection (Rolli *et al.*, 2018; Righetti *et al.*, 2019). In our maize–AFB1 system, we observed a strong difference between treated and untreated plantlets, and most relevant metabolic responses were observed in roots; this is not surprising, considering the higher exposure of such organs to AFB1. On the other hand, AFB1-induced stress was significantly lowered in stem and leaf, consistent with the assumption of compartmentalized metabolism in plants, among different organs, but suggesting an influence in the overall defensive strategy of maize.

According to our untargeted metabolomics investigation, anthocyanin biosynthesis and chlorophyll metabolism in roots are most affected. The biosynthesis of these metabolites seems to be inhibited by AFB1 accumulation. Both anthocyanin and chlorophylls were exclusively found in control roots, exhibiting a tissue-specific accumulation. Such a phenomenon may be related to a scarcely explored hypothesis, suggesting that at least in *Z. mays* (McLean *et al.*, 1992) and *Nicotiana tabacum* (McLean *et al.*, 1995), aflatoxins may interfere with the normal functioning of chloroplasts. The inhibition of chlorophyll synthesis is reported to be more pronounced with increasing concentrations of AFB1. At a higher dose (25 μg ml^{-1}), *Nicotiana tabacum* plantlets are also reported to fail to develop roots, following 3 weeks of exposure. This will depend on the developmental stage at which a plant is likely to be exposed to the toxin, i.e. in the developing seed (likely to be more sensitive) or in plants that are already established (likely to be less sensitive). Similarly, in the interplay between plants and fungi, inoculation of plantlets with fungi has been involved in the repression of anthocyanin biosynthesis, with the blockage of genes encoding key enzymes involved in the production of these secondary metabolites, such as flavanone 3-hydroxylase, dihydroflavonol 4-reductase and anthocyanidin synthase (Lo and Nicholson, 1998).

In plants, chloroplast development is regulated by cytokinin molecules. Recently, it was revealed that the cytokinin signaling pathway is also involved in the regulation of chloroplast development in the root, through the upregulation of transcription factor (golden2-like) in non-photosynthetic organs (Kobayashi *et al.*, 2012). These phytohormones are key regulators of many aspects of plant development and may mediate plant stress responses, including anthocyanin accumulation (Deikman and Hammer, 1995). In this study, several anthocyanins were found to be exclusively located in the root cortex of untreated maize, and their presence was inhibited by AFB1 exposure. These results may suggest a possible involvement of aflatoxins in mediating a hormone-like response, through the inhibition of the cytokinin signaling pathway, resulting, among other effects, in the alteration of chlorophyll metabolism and the inhibition of anthocyanin biosynthesis. It remains to be determined whether these effects are the result of a metabolic response elicited by AFB1, with maize repressing less essential metabolic activities as a means of compensating for future defensive response needs, or a direct hacking/toxic activity against plant physiology. Involvement as a virulence factor cannot be excluded, however.

Indeed, conversely to what has been thought previously, there is growing evidence that in certain situations several mycotoxins, including alternariol, DON and gliotoxin, may play a role in facilitating the growth and spread of fungi in the host plant (Hof, 2008; Wenderoth *et al.*, 2019).

This assumption is also supported by evidence at the protein level, corroborating the hypothesis of an interaction between phytohormones, such as cytokinins (Chen *et al.*, 2010), with a pathogenesis-related protein (i.e. PR10) induced in an aflatoxin-resistant maize line (Chen *et al.*, 2010). Indeed, several constitutively expressed maize proteins were reported to have a role as the first line of defense against aflatoxin (Chen *et al.*, 2010), including the biosynthesis of thioredoxin, which regulates various biological processes during chloroplast development (i.e. synthesis of chlorophylls and assembly of photosynthetic protein–cofactor complexes) (Buchanan and Balmer, 2005).

On the other hand, metabolites found in above-ground organs suggest that the plant may react to the presence of AFB1 in the same way as it reacts during fungal infection. Indeed, several plant secondary metabolites known for their antimicrobial or antioxidant activities (i.e. flavonoids, phenylpropanoid, hydroxycinnamic acids, alkylresorcinols) have been previously reported to be differentially modulated in the presence of mycotoxins (i.e. DON) (Gunnaiah and Kushalappa, 2014; Etzerodt *et al.*, 2016). In response to AFB1 treatment, we identified some benzoxazinoids compounds previously reported to inhibit DON accumulation (Etzerodt *et al.*, 2016) in wheat cultivars. These compounds are considered as phytoanticipins, and given their defensive role, HDMBOA-Glc accumulated in the outer leaf sheath of the AFB1-treated stem may be produced in advance to face a potential fungal attack, as anticipated from the limited level of aflatoxins (Ahmad *et al.*, 2011).

A different class of phytohormones, namely brassinosteroids, were found to be modulated in maize as a response to AFB1. Indeed, deoxybrassinolide, found to be accumulated in the outer leaf sheath of the treated stem, is known to have protective effects on growth, chlorophyll biosynthesis and membrane stability in maize (He *et al.*, 1991; Katsumi, 1991). Recently, the critical role of brassinosteroids in the regulation of xenobiotic metabolism in crop plants was revealed (Zhou *et al.*, 2015). The authors reported that their physiological concentration is capable to upregulate the machinery of the detoxifying response against pesticides, mostly mediated by the activity of glutathione *S*-transferase (Zhou *et al.*, 2015). Therefore, the increased biosynthesis of brassinosteroids, noted in treated plantlets, should be considered as a first step towards the activation of a defensive system in the detoxifying strategy of maize against mycotoxins.

In summary, our results suggest a possible role of AFB1 in maize pathogenesis, supporting the hypothesis that the production and the environmental exposure of certain mycotoxins may increase pathogen virulence or act as an alert system for maize plantlets.

Overall, major metabolism disruption was observed in roots, with significant interference with chlorophyll and anthocyanin biosynthesis, which may potentially be ascribable to cytokinin pathway inhibition. On the other hand, a smaller effect was observed in the leaf chloroplast, which is the photosynthetic organ, because the quantity of AFB1 translocated to the leaves was not enough to exert phytotoxicity. The *in vitro* plant system used could help in investigating the phytotoxicity mechanism that should then be translated to the open field scenario. Indeed, the fungal infestation occurs in the aerial part of the plant, leading to an accumulation of aflatoxin in the leaf and the potential consequent disruption of chloroplast metabolism in the photosynthetic organ. The natural reservoir of *Fusarium* and mycotoxigenic fungi is, however, represented by the soil, and their large presence in the rhizosphere may determine a higher exposure via root uptake (Edel-Hermann *et al.*, 2015). This may pave the way to above-ground infections by weakening the plant defensive system or elicit the biochemical immune response of maize itself by increasing phytoanticipin and phytoalexin biosynthesis.

A more detailed molecular characterization of the mechanism of phytotoxicity of aflatoxins is necessary to confirm the putative role and crosstalk of cytokinin-signaling pathways in the defense response of maize. The integration of different omics techniques is necessary to acquire the big picture of the multifactorial mechanism of plant resistance, which could be useful as a breeding target for the control of mycotoxins in cereals and may help to further elucidate the intricate chemical interplay between plants and other organisms.

EXPERIMENTAL PROCEDURES

Chemicals

AFB1 (2 mg L^{-1} in acetonitrile) was obtained from Romer Labs (https://www.romerlabs.com) and AFM2 (100 μg) was obtained from Tebu-Bio (https://www.tebu-bio.com). 2,5-Dihydroxybenzoic acid (DHB), α-cyano-4-hydroxycinnamic acid (CHCA), trifluoroacetic acid (TFA), MilliQ water, MS-grade acetone and acetonitrile were purchased from Sigma-Aldrich (https://www.sigmaaldrich.com). Gelatin, used for embedding, was obtained from VWR International (https://www.vwr.com). Glass microscope slides (ground edges, super frost) were obtained from R. Langenbrinck (http://www.langenbrinck.com).

Plant material and growth conditions

Belgrano maize (*Z. mays*) hybrid (FAO class 300) seeds were germinated to obtain plantlets as previously reported (Righetti *et al.*, 2017; Rolli *et al.*, 2018). Briefly, plants were placed for 7 and 14 days in a glass jar containing Murashige and Skoog medium, spiked with 200 μg of AFB1. The experiment time was previously optimized to avoid the occurrence of visual symptoms in the control experiments (i.e. leaf senescence). Liquid medium without

mycotoxin was used in all experiments as a control. All the experiments were carried out in triplicate. Immediately after sampling, 20-mm segments of roots, stems and leaves were obtained by transverse cuts with a scalpel (Figure S14).

Evaluation of MALDI matrices for mycotoxins

The dried-droplet method of sample application was initially used to assess the matrices of CHCA (5 mg ml^{-1}) and DHB (30 mg ml^{-1}), by mixing 1 μl of AFB1 standard with 1 μl of matrix solution and spotting 0.5 μl onto 80-well stainless-steel plates.

Sample preparation

Sample preparation for MALDI was performed following a previously optimized protocol (Bhandari *et al.*, 2015). Briefly, fresh samples were embedded in 2% (w/v) gelatin solution in a cryo-mold and then 20-μm-thick sections were cut at −20°C using a cryomicrotome (HM525 cryostat; ThermoFisher Scientific, https://www.thermofisher.com). The sections were transferred to a glass slide and kept at −80°C until the day of analysis. Before matrix application, optical images of the sections were taken, using a digital microscope (VHX-5000; KEYENCE, https://www.keyence.com). DHB (30 mg ml^{-1}) in acetone:water (50:50, v/v, 0.1% TFA) was chosen as a matrix and sprayed using an automated pneumatic sprayer system (SMALDIPrep; TransMIT, https://www.transmit.de) (Bouschen *et al.* 2010) to ensure the uniform coating of tissue sections with microcrystalline matrix. The size and uniformity of the deposited crystals were checked prior to AP-SMALDI MSI experiments. At least two biological replicates of each tissue (i.e. root, stem and leaf) were analyzed by MSI.

AP-SMALDI MSI analysis

Plant tissue section imaging experiments were performed using a high spatial resolution (≥5 μm laser spot size) atmospheric pressure scanning microprobe matrix-assisted laser desorption/ionization MSI ion source (AP-SMALDI5 AF; TransMIT) coupled to a Q Exactive HF orbital trapping mass spectrometer (ThermoFisher Scientific).

The minimum laser-beam focus results in an ablation spot diameter of 5 μm (Römpp *et al.* 2010, Römpp *et al.*, 2013). For the experiments described below, laser step sizes between 5 and 30 μm were set, depending on the tissue under investigation. The mass spectrometer was operated in positive-ion mode. The following parameters were set: scan range, m/z = 250–1000; spray voltage, +3 kV; capillary temperature, 250°C; automatic gain control (AGC) was disabled; cycle time for one pixel was 1 s in pixelated mode at a mass resolution of 240 000 at an m/z of 200. Internal mass calibration was performed using known matrix ion signals as lock mass values (m/z 716.12462), providing a mass accuracy of better than 2 ppm root-mean-square error over the entire measurement. High-resolution (HR) AP-SMALDI MS/MS analysis was performed on a tissue section prepared identically to that used for MSI, if the ion intensities were high enough. Furthermore, UHPLC HRMS/MS analysis was performed on maize extract to confirm the identity of the metabolites investigated in the present study. The sample extraction method and HRMS/MS detection parameters are summarized in Appendix S1.

Data processing and image generation

Raw data (imzML format) were imported and processed using LIPOSTARMSI (Tortorella *et al.*, 2020). Descriptions of user data import and identification parameters are provided in Table S1. Exploratory data analysis was applied to mine complex MSI datasets using both bisection k-means segmentation analysis and PCA (Kulkarni *et al.*, 2018). Segmentation was performed via bisecting k-means with spatial de-noise data processing and with total ion current (TIC) normalization (Alexandrov *et al.*, 2011, Alexandrov, 2012). Based on plant tissue compartmentalization suggested by exploratory data analysis (PCA, bisecting k-means), ROIs were manually defined, average spectra calculated with an m/z tolerance of 2 ppm and multivariate statistical analysis (i.e. PCA) was performed. A background ROI for each sample was created and used to subtract all ions generated from the matrix. Metabolite annotation of MSI data was performed against publically available LIPID MAPS and PlantCyc databases by accurate m/z matching within user-set tolerances. Metabolite identification was completed by checking the HRMS/MS spectra (when available) and following the guidelines made by Schymanski *et al.* (2014).

Ion images of selected m/z values were generated with an m/z bin width of ±2 ppm and normalized to TIC. To better visualize the localization of selected metabolites, TIC images for each data set were calculated and used to semi-automatically (by using two arbitrary teaching points on the high-resolution and TIC image) co-register with corresponding high-resolution images.

Raw data were deposited on the METASPACE platform (https://metaspace2020.eu) (Palmer *et al.*, 2017).

DATA AVAILABILITY STATEMENT

Mass spectrometry imaging data that support the findings of this study have been deposited in METASPACE (https://metaspace2020.eu/datasets) with the accession codes JLU Giessen_ Wroot_llreplicate_llmeasur_296x151_10um_A20, MS_crt_AFB1_338x172_30um_A_20_FP, MF_control_454x160_10um_A20 and ML_AFB1_123x468_10um_A20.

ACKNOWLEDGMENTS

LR acknowledges the German–Italian Research Short-Term Scholarship (DAAD-2019, ID:91714320) funded by the German Academic Exchange Service (DAAD). Financial support by the Deutsche Forschungsgemeinschaft (DFG) under grant Sp314/13-1 and INST 162/500-1 FUGG is gratefully acknowledged. Open Access funding enabled and organized by ProjektDEAL.

AUTHOR CONTRIBUTIONS

LR conceived the study, performed sample preparations and AP-SMALDI MSI experiments, discussed results and wrote the article. DRB supported sample preparations and AP-SMALDI MSI experiments, data analysis and data evaluation. ER designed and performed micropropagation experiments. ST contributed to statistical analysis using LIPOSTARMSI. RB supported data evaluation, and contributed to data discussion and drafting. CD and BS provided the methodology and funding, supervised the project and critically revised the article for important intellectual content. All of the authors contributed to data discussion, according to their multidisciplinary expertise.

CONFLICT OF INTEREST

BS is a consultant and DB is a part-time employee of TransMIT GmbH, Giessen, Germany. The other authors declare that they have no conflicts of interest.

SUPPORTING INFORMATION

Additional Supporting Information may be found in the online version of this article.

Figure S1. Residual AFB1 in the growing medium and its distribution in plant organs.

Figure S2. Optical image of a root cross section.

Figure S3. HRMS/MS spectrum of AFM2.

Figure S4. Principal component analysis score plots built using the ROI resulting from the segmentation analysis for root.

Figure S5. Co-localization of different adducts of pheophytin a.

Figure S6. In-tissue HRMS/MS spectrum of protonated species of pheophytin a and pheophytin b.

Figure S7. Spatial distribution of anthocyanidins in root organ.

Figure S8. Malvidin spatial distribution in maize roots.

Figure S9. Exploratory data analysis for AP-SMALDI imaging of a maize stem sample to visualize inter- and intrasample comparison.

Figure S10. Principal component analysis score plots built using the ROI resulting from the segmentation analysis for the stem.

Figure S11. Additional metabolites associated with stem defense against AFB1 accumulation uncovered by AP-SMALDI MSI.

Figure S12. Exploratory data analysis for AP-SMALDI MSI maize leaf samples.

Figure S13. Principal component analysis score plots built using the ROI resulting from the segmentation analysis for leaf samples.

Figure S14. Illustration of the root, stem and leaf segments used in this study.

Appendix S1. Sample preparation and UHPLC-HRMS/MS analysis.

Table S1. Data import MSI processing settings.

Table S2. List of metabolites imaged in maize organs based and differentially accumulated in control versus AFB1-treated plantlets.

REFERENCES

Accinelli, C., Abbas, H.K., Zablotowicz, R.M. & Wilkinson, J.R. (2008) Aspergillus flavus aflatoxin occurrence and expression of aflatoxin biosynthesis genes in soil. *Can. J. Microbiol.* **54**, 371–379. Available at: http://www.nrcresearchpress.com/doi/10.1139/W08-018

Ahmad, S., Veyrat, N., Gordon-Weeks, R. *et al.* (2011) Benzoxazinoid metabolites regulate innate immunity against aphids and fungi in maize. *Plant Physiol.* **157**, 317–327. Available at: http://www.plantphysiol.org/lookup/doi/10.1104/pp.111.180224

Alexandrov, T. & Kobarg, J.H. (2011) Efficient Spatial Segmentation of Large Imaging Mass Spectrometry Datasets with Spatially Aware Clustering. *Bioinformatics*, **27**(13), i230–i238. https://doi.org/10.1093/bioinformatics/btr246.

Alexandrov, T. (2012) MALDI Imaging Mass Spectrometry: Statistical Data Analysis and Current Computational Challenges. *BMC Bioinf*, **13**(Suppl 16), S11. https://doi.org/10.1186/1471-2105-13-S16-S11.

Bártíková, H., Skálová, L., Stuchíková, L., Vokřál, I., Vaněk, T. & Podlipná, R. (2015) Xenobiotic-metabolizing enzymes in plants and their role in uptake and biotransformation of veterinary drugs in the environment. *Drug Metab. Rev.* **47**, 374–387.

Berthiller, F., Crews, C., Dall'Asta, C. *et al.* (2013) Masked mycotoxins: a review. *Mol. Nutr. Food Res.* **57**, 165–186. Available at: http://doi.wiley.com/10.1002/mnfr.201100764

Bhandari, D.R., Wang, Q., Friedt, W., Spengler, B., Gottwald, S. & Römpp, A. (2015) High resolution mass spectrometry imaging of plant tissues: towards a plant metabolite atlas. *Analyst*, **140**, 7696–7709. Available at: http://xlink.rsc.org/?DOI=C5AN01065A

Bhandari, D.R., Wang, Q., Li, B., Friedt, W., Römpp, A., Spengler, B. & Gottwald, S. (2018) Histology-guided high-resolution AP-SMALDI mass spectrometry imaging of wheat-Fusarium graminearum interaction at the root–shoot junction. *Plant Methods*, **14**, 103. Available at: https://plantmethods.biomedcentral.com/articles/10.1186/s13007-018-0368-6

Biedrzycki, M.L. & Bais, H.P. (2010) Kin recognition: another biological function for root secretions. *Plant Signal. Behav.* **5**, 401–402. Available at: http://www.tandfonline.com/doi/abs/10.4161/psb.5.4.10795

Bjarnholt, N., Li, B., D'Alvise, J. & Janfelt, C. (2014) Mass spectrometry imaging of plant metabolites – principles and possibilities. *Nat. Prod. Rep.* **31**, 818–837. Available at: http://xlink.rsc.org/?DOI=C3NP70100J

Bonfante, P. & Genre, A. (2010) Mechanisms underlying beneficial plant–fungus interactions in mycorrhizal symbiosis. *Nat. Commun.* **1**, 48. Available at: http://www.nature.com/articles/ncomms1046

Boughton, B.A., Thinagaran, D., Sarabia, D., Bacic, A. & Roessner, U. (2016) Mass spectrometry imaging for plant biology: a review. *Phytochem. Rev.* **15**, 445–488. Available at: http://link.springer.com/10.1007/s11101-015-9440-2

Bouschen, W., Schulz, O., Eikel, D. & Spengler, B. (2010) Rapid Commun. *Mass Spectrom*, **24**, 355–364.

Buchanan, B.B. & Balmer, Y. (2005) REDOX REGULATION: A Broadening Horizon. *Annu. Rev. Plant Biol.* **56**, 187–220. Available at: http://www.annualreviews.org/doi/10.1146/annurev.arplant.56.032604.144246

Buer, C.S., Muday, G.K. & Djordjevic, M.A. (2007) Flavonoids are differentially taken up and transported long distances in Arabidopsis. *Plant Physiol.* **145**, 478–490. Available at: http://www.plantphysiol.org/lookup/doi/10.1104/pp.107.101824

Chen, D., Wang, S., Qi, L., Yin, L. & Deng, X. (2018) Galactolipid remodeling is involved in drought-induced leaf senescence in maize. *Environ. Exp. Bot.* **150**, 57–68. Available at: https://linkinghub.elsevier.com/retrieve/pii/S0098847218303198

Chen, Z.-Y., Brown, R.L., Damann, K.E. & Cleveland, T.E. (2010) PR10 expression in maize and its effect on host resistance against Aspergillus flavus infection and aflatoxin production. *Mol. Plant Pathol.* **11**, 69–81. Available at: http://doi.wiley.com/10.1111/j.1364-3703.2009.00574.x

Coleman, J., Blake-Kalff, M. & Davies, E. (1997) Detoxification of xenobiotics by plants: chemical modification and vacuolar compartmentation. *Trends Plant Sci.* **2**, 144–151. https://linkinghub.elsevier.com/retrieve/pii/S1360138597010194

Crush, J.R., Briggs, L.R., Sprosen, J.M. & Nichols, S.N. (2008) Effect of irrigation with lake water containing microcystins on microcystin content and growth of ryegrass, clover, rape, and lettuce. *Environ. Toxicol.* **23**, 246–252. Available at: http://doi.wiley.com/10.1002/tox.20331

D'Abrosca, B., Scognamiglio, M., Fiumano, V., Esposito, A., Choi, Y.H., Verpoorte, R. & Fiorentino, A. (2013) Plant bioassay to assess the effects of allelochemicals on the metabolome of the target species Aegilops geniculata by an NMR-based approach. *Phytochemistry*, **93**, 27–40. Available at: https://linkinghub.elsevier.com/retrieve/pii/S003194221300112X

van Dam, N.M. & Bouwmeester, H.J. (2016) Metabolomics in the rhizosphere: tapping into belowground chemical communication. *Trends Plant Sci.* **21**, 256–265. Available at: https://linkinghub.elsevier.com/retrieve/pii/S1360138516000091

Deikman, J. & Hammer, P.E. (1995) Induction of anthocyanin accumulation by cytokinins in Arabidopsis thaliana. *Plant Physiol.* **108**, 47–57. Available at: http://www.plantphysiol.org/lookup/doi/10.1104/pp.108.1.47

Dueñas, M.E., Klein, A.T., Alexander, L.E., Yandeau-Nelson, M.D., Nikolau, B.J. & Lee, Y.J. (2017) High spatial resolution mass spectrometry imaging reveals the genetically programmed, developmental modification of the distribution of thylakoid membrane lipids among individual cells of maize leaf. *Plant J.* **89**, 825–838. Available at: http://doi.wiley.com/10.1111/tpj.13422

Edel-Hermann, V., Gautheron, N., Mounier, A. & Steinberg, C. (2015) Fusarium diversity in soil using a specific molecular approach and a cultural approach. *J. Microbiol. Methods*, **111**, 64–71. Available at: https://linkinghub.elsevier.com/retrieve/pii/S0167701215000408

Etzerodt, T., Gislum, R., Laursen, B.B., Heinrichson, K., Gregersen, P.L., Jørgensen, L.N. & Fomsgaard, I.S. (2016) Correlation of Deoxynivalenol Accumulation in Fusarium-Infected Winter and Spring Wheat Cultivars with Secondary Metabolites at Different Growth Stages. *J. Agric. Food Chem.* **64**, 4545–4555. Available at: https://pubs.acs.org/doi/10.1021/acs.jafc.6b01162

Figueroa, M., Manning, V.A., Pandelova, I. & Ciuffetti, L.M. (2015) Persistence of the Host-Selective Toxin Ptr ToxB in the Apoplast. *Mol. Plant-Microbe Interact.* **28**, 1082–1090. Available at: http://apsjournals.apsnet.org/doi/10.1094/MPMI-05-15-0097-R

Gunnaiah, R. & Kushalappa, A.C. (2014) Metabolomics deciphers the host resistance mechanisms in wheat cultivar Sumai-3, against trichothecene producing and non-producing isolates of Fusarium graminearum. *Plant Physiol. Biochem.* **83**, 40–50. Available at: https://linkinghub.elsevier.com/retrieve/pii/S0981942814002150

Hariprasad, P., Vipin, A.V., Karuna, S., Raksha, R.K. & Venkateswaran, G. (2015) Natural aflatoxin uptake by sugarcane (Saccharum officinaurum L.) and its persistence in jaggery. *Environ. Sci. Pollut. Res.* **22**, 6246–6253. Available at: http://link.springer.com/10.1007/s11356-014-3851-2

He, R., Wang, G. & Wang, X. (1991) Effects of Brassinolide on Growth and Chilling Resistance of Maize Seedlings. 220–230. Available at: https://pubs.acs.org/doi/abs/10.1021/bk-1991-0474.ch019

Herzig, R., Bieri, C., Weber, A. & Straehl, P. (2011) Organic Xenobiotics and Plants. P. Schröder and C. D. Collins, eds., Dordrecht: Springer, Netherlands. Available at: http://link.springer.com/10.1007/978-90-481-9852-8

Hickert, S., Cramer, B., Letzel, M.C. & Humpf, H.-U. (2016) Matrix-assisted laser desorption/ionization time-of-flight mass spectrometry imaging of ochratoxin A and fumonisins in mold-infected food. *Rapid Commun. Mass Spectrom.* **30**, 2508–2516. Available at: http://doi.wiley.com/10.1002/rcm.7733

Hof, H. (2008) Mycotoxins: pathogenicity factors or virulence factors? *Mycoses*, **51**, 93–94.

Ismaiel, A.A. & Papenbrock, J. (2015) Mycotoxins: producing fungi and mechanisms of phytotoxicity. *Agriculture*, **5**, 493–537.

Jachetta, J.J., Appleby, A.P. & Boersma, L. (1986) Apoplastic and symplastic pathways of atrazine and glyphosate transport in shoots of seedling sunflower. *Plant Physiol.* **82**, 1000–1007. Available at: http://www.plantphysiol.org/lookup/doi/10.1104/pp.82.4.1000

Jones, D.L., Nguyen, C. & Finlay, R.D. (2009) Carbon flow in the rhizosphere: carbon trading at the soil-root interface. *Plant Soil*, **321**, 5–33.

Katsumi, M. (1991) Physiological Modes of Brassinolide Action in Cucumber Hypocotyl Growth. 246–254. Available at: https://pubs.acs.org/doi/abs/10.1021/bk-1991-0474.ch021

Kobayashi, K., Baba, S., Obayashi, T. *et al.* (2012) Regulation of root greening by light and auxin/cytokinin signaling in Arabidopsis. *Plant Cell*, **24**, 1081–1095.

Kulkarni, P., Dost, M., Bulut, Ö.D., Welle, A., Böcker, S., Boland, W. & Svatoš, A. (2018) Secondary ion mass spectrometry imaging and multivariate data analysis reveal co-aggregation patterns of Populus trichocarpa leaf surface compounds on a micrometer scale. *Plant J.* **93**, 193–206. Available at: http://doi.wiley.com/10.1111/tpj.13763

Llewellyn, G.C., Reynolds, J.D., Hurst, L., Vance, R.A. & Dashek, W.V. (1982) Uptake of Zn++ and aflatoxin from perlite and liquid culture by Zea mays seedlings. *Mycopathologia*, **77**, 111–116. Available at: http://link.springer.com/10.1007/BF00437393

Lo, S.-C.-C. & Nicholson, R.L. (1998) Reduction of Light-Induced Anthocyanin Accumulation in Inoculated Sorghum Mesocotyls. *Plant Physiol.* **116**, 979–989. Available at: http://www.plantphysiol.org/lookup/doi/10.1104/pp.116.3.979

Martin, R.A. & Edgington, L.V. (1981) Comparative systemic translocation of several xenobiotics and sucrose. *Pestic. Biochem. Physiol.* **16**, 87–96.

McLean, M., Berjak, P., Watt, M.P. & Dutton, M.F. (1992) The effects of aflatoxin B1 on immature germinating maize (Zea mays) embryos. *Mycopathologia*, **119**, 181–190. Available at: http://link.springer.com/10.1007/BF00448817

McLean, M., Watt, M.P., Berjak, P. & Dutton, M.F. (1995) Aflatoxin B 1 —its effects on an in vitro plant system. *Food Addit. Contam.* **12**, 435–443. Available at: http://www.tandfonline.com/doi/abs/10.1080/02652039509374327

Meinzer, F.C. & Moore, P.H. (1988) Effect of apoplastic solutes on water potential in elongating sugarcane leaves. *Plant Physiol.* **86**, 873–879.

Mertz, D., Lee, D., Zuber, M. & Lillehoj, E. (1980) Uptake and metabolism of aflatoxin by Zea mays. *J. Agric. Food Chem.* **28**, 963–966. Available at: https://pubs.acs.org/doi/abs/10.1021/jf60231a003

Nelson, D.R. (2006) Plant cytochrome P450s from moss to poplar. *Phytochem. Rev.* **5**, 193–204. Available at: http://link.springer.com/10.1007/s11101-006-9015-3

de Oliveira, D.N., Ferreira, M.S. & Catharino, R.R. (2014) Rapid and Simultaneous In Situ Assessment of Aflatoxins and Stilbenes Using Silica Plate Imprinting Mass Spectrometry Imaging J. Koomen, M., ed). *PLoS One*, **9**, e90901. Available at: https://dx.plos.org/10.1371/journal.pone.0090901

Palmer, A., Phapale, P., Chernyavsky, I. *et al.* (2017) FDR-controlled metabolite annotation for high-resolution imaging mass spectrometry. *Nat. Methods*, **14**, 57–60. Available at: http://www.nature.com/articles/nmeth.4072

Perincherry, L., Lalak-Kańczugowska, J. & Stępień, Ł. (2019) Fusarium-Produced Mycotoxins in Plant-Pathogen Interactions. *Toxins*, **11**(11), 2072–6651. Available at: https://www.mdpi.com/2072-6651/11/11/664

Peuthert, A., Chakrabarti, S. & Pflugmacher, S. (2007) Uptake of microcystins-LR and -LF (cyanobacterial toxins) in seedlings of several important agricultural plant species and the correlation with cellular damage (lipid peroxidation). *Environ. Toxicol.* **22**, 436–442. Available at: http://doi.wiley.com/10.1002/tox.20266

Proctor, R.H., Desjardins, A.E., McCormick, S.P., Plattner, R.D., Alexander, N.J. & Brown, D.W. (2002) Genetic analysis of the role of trichothecene and fumonisin mycotoxins in the virulence of Fusarium. *Eur. J. Plant Pathol.* **108**, 691–698.

Righetti, L., Körber, T., Rolli, E., Galaverna, G., Suman, M., Bruni, R. & Dall'Asta, C. (2019) Plant biotransformation of T2 and HT2 toxin in cultured organs of Triticum durum Desf. *Sci. Rep.* **9**(1), 1–11.

Righetti, L., Rolli, E., Galaverna, G., Suman, M., Bruni, R. & Dall'Asta, C. (2017) Plant organ cultures as masked mycotoxin biofactories: Deciphering the fate of zearalenone in micropropagated durum wheat roots and leaves. *PLoS One*, **12**(11), e0187247. Available at: https://dx.plos.org/10.1371/journal.pone.0187247

Rolli, E., Righetti, L., Galaverna, G., Suman, M., Dall'Asta, C. & Bruni, R. (2018) Zearalenone uptake and biotransformation in Micropropagated Triticum durum Desf. Plants: a xenobolomic approach. *J. Agric. Food Chem.* **66**, 1523–1532.

Römpp, A., Guenther, S., Schober, Y., Schulz, O., Takats, Z., Kummer, W. & Spengler, B. (2010) Angew. Chem. *Int. Ed.*, **49**, 3834–3838.

Römpp, A. & Spengler, B. (2013) Histochem. *Cell Biol.* **139**, 759–783.

Rychlik, M., Humpf, H.-U., Marko, D., Dänicke, S., Mally, A., Berthiller, F., Klaffke, H. & Lorenz, N. (2014) Proposal of a comprehensive definition of modified and other forms of mycotoxins including "masked" mycotoxins. *Mycotoxin Res.* **30**, 197–205. Available at: http://link.springer.com/10.1007/s12550-014-0203-5

Salinas Moreno, Y., Sanchez, G.S., Hernandez, D.R. & Lobato, N.R. (2005) Characterization of anthocyanin extracts from maize kernels. *J. Chromatogr. Sci.* **43**, 483–487. Available at: https://academic.oup.com/chromsci/article-lookup/doi/10.1093/chromsci/43.9.483

Schröder, P. & Collins, C. (2002) Conjugating enzymes involved in xenobiotic metabolism of organic xenobiotics in plants. *Int. J. Phytoremediation*, **4**, 247–265. Available at: http://www.tandfonline.com/doi/abs/10.1080/15226510208500086

Schulz, M., Marocco, A., Tabaglio, V., Macias, F.A. & Molinillo, J.M.G. (2013) Benzoxazinoids in Rye Allelopathy - From Discovery to Application in Sustainable Weed Control and Organic Farming. *J. Chem. Ecol.* **39**, 154–174. Available at: http://link.springer.com/10.1007/s10886-013-0235-x

Schymanski, E.L., Jeon, J., Gulde, R., Fenner, K., Ruff, M., Singer, H.P. & Hollender, J. (2014) Identifying Small Molecules via High Resolution Mass Spectrometry: Communicating Confidence. *Environ. Sci. Technol.* **48**, 2097–2098. https://doi.org/10.1021/es5002105.

Siminszky, B. (2006) Plant cytochrome P450-mediated herbicide metabolism. *Phytochem. Rev.* **5**, 445–458. Available at: http://link.springer.com/10.1007/s11101-006-9011-7

Snigdha, M., Hariprasad, P. & Venkateswaran, G. (2015) Transport via xylem and accumulation of aflatoxin in seeds of groundnut plant. *Chemosphere*, **119**, 524–529. Available at: https://linkinghub.elsevier.com/retrieve/pii/S0045653514008947

Tenenboim, H. & Brotman, Y. (2016) Omic relief for the biotically stressed: metabolomics of plant biotic interactions. *Trends Plant Sci.* **21**, 781–791. Available at: https://linkinghub.elsevier.com/retrieve/pii/S1360138516300267

Tortorella, S., Tiberi, P., Bowman, A.P., Claes, B.S.R., Ščupáková, K., Heeren, R.M.A., Ellis, S.R. & Cruciani, G. (2020) LipostarMSI: Comprehensive, Vendor-Neutral Software for Visualization, Data Analysis, and Automated Molecular Identification in Mass Spectrometry Imaging. *J. Am. Soc. Mass Spectrom.* **31**, 155–163. Available at: https://pubs.acs.org/doi/10.1021/jasms.9b00034

Venturi, V. & Keel, C. (2016) Signaling in the Rhizosphere. *Trends Plant Sci.* **21**, 187–198. Available at: https://linkinghub.elsevier.com/retrieve/pii/S1360138516000066

Villette, C., Maurer, L., Wanko, A. & Heintz, D. (2019) Xenobiotics metabolization in Salix alba leaves uncovered by mass spectrometry imaging. *Metabolomics*, **15**, 122. Available at: http://link.springer.com/10.1007/s11306-019-1572-8

Walker, S.J., Llewellyn, G.C., Lillehoj, E.B. & Dashek, W.V. (1984) Uptake and subcellular distribution of aflatoxin B1 by excised, cultured soybean roots and toxin effects on root elongation. *Environ. Exp. Bot.* **24**, 113–122. Available at: https://linkinghub.elsevier.com/retrieve/pii/0098847284900121

Wenderoth, M., Garganese, F., Schmidt-Heydt, M., Soukup, S.T., Ippolito, A., Sanzani, S.M. & Fischer, R. (2019) Alternariol as virulence and colonization factor of Alternaria alternata during plant infection. *Mol. Microbiol.* **112**, 131–146. Available at: https://onlinelibrary.wiley.com/doi/abs/10.1111/mmi.14258

Wipfler, R., McCormick, S.P., Proctor, R., Teresi, J., Hao, G., Ward, T., Alexander, N. & Vaughan, M.M. (2019) Synergistic phytotoxic effects of culmorin and trichothecene mycotoxins. *Toxins (Basel)*, **11**, 555. Available at: https://www.mdpi.com/2072-6651/11/10/555

Zhalnina, K., Louie, K.B., Hao, Z. *et al.* (2018) Dynamic root exudate chemistry and microbial substrate preferences drive patterns in rhizosphere microbial community assembly. *Nat. Microbiol.* **3**, 470–480. Available at: http://www.nature.com/articles/s41564-018-0129-3

Zhang, Z., Nie, D., Fan, K., Yang, J., Guo, W., Meng, J., Zhao, Z. & Han, Z. (2019) A systematic review of plant-conjugated masked mycotoxins: occurrence, toxicology, and metabolism. *Crit. Rev. Food Sci. Nutr.* **60**(9), 1523–1537. Available at: https://www.tandfonline.com/doi/full/10.1080/10408398.2019.1578944

Zhou, S., Richter, A. & Jander, G. (2018) Beyond defense: multiple functions of benzoxazinoids in maize metabolism. *Plant Cell Physiol.* **59**, 1528–1537. Available at: https://academic.oup.com/pcp/article/59/8/1528/4951958

Zhou, Y., Xia, X., Yu, G. *et al.* (2015) Brassinosteroids play a critical role in the regulation of pesticide metabolism in crop plants. *Sci. Rep.* **5**, 9018. Available at: http://www.nature.com/articles/srep09018